

# New Pressure Stabilization Structure in Two-Dimensional PtSe<sub>2</sub>

Kai Jiang,<sup>†</sup> Anyang Cui,<sup>†</sup> Sen Shao,<sup>†</sup> Jiajia Feng, Hongliang Dong, Bin Chen, Yanchao Wang,\*  
Zhigao Hu,\* and Junhao Chu



Cite This: *J. Phys. Chem. Lett.* 2020, 11, 7342–7349



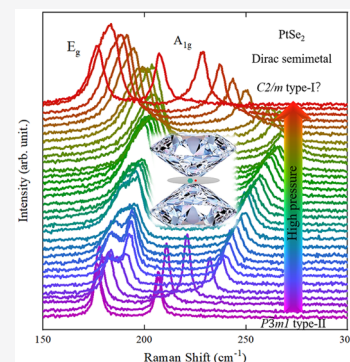
Read Online

ACCESS |

Metrics & More

Article Recommendations

**ABSTRACT:** The frequency shifts and lattice dynamics to unveil the vibrational properties of platinum diselenide (PtSe<sub>2</sub>) are investigated using pressure-dependent polarized Raman scattering at room temperature up to 25 GPa. The two phonon modes E<sub>g</sub> and A<sub>1g</sub> display similar hardening trends; both the Raman peak positions and full widths at half-maximum have distinct mutation phenomena under high pressure. Especially, the split E<sub>g</sub> mode at 4.3 GPa confirms the change of the lattice symmetry. With the aid of the first-principles calculations, a new pressure stabilization structure C2/m of PtSe<sub>2</sub> has been found to be in good agreement with experiments. The band structures calculations reveal that the new phase is a novel type-I Dirac semimetal. The results demonstrate that the pressure-dependent Raman spectra combined with theoretical predictions may open a new window for searching and controlling the phase structure and Dirac cones of two-dimensional materials.



Recently, layered transition metal dichalcogenides (TMDs) have been in the spotlight of the research community because of their physical properties and promising potential applications in the field of electronics and optoelectronics.<sup>1–6</sup> Platinum diselenide (PtSe<sub>2</sub>) has emerged as an interesting compound that belongs to TMDs and predicted the highest phonon limited electron mobility among the previous studied TMDs materials at room temperature.<sup>7,8</sup> In particular, PtSe<sub>2</sub> has proved to be an attractive candidate for a variety of applications due to its unique electronic property whereby theoretical studies proposed a transition from semimetal to semiconductor by controlling the layer numbers.<sup>9–11</sup> Recently, both theoretical predictions and experimental results have confirmed that bulk 1T-PtSe<sub>2</sub> is a novel type-II Dirac semimetal.<sup>12–16</sup> Previous study has shown that the type-II Dirac Fermions protected by C<sub>3</sub> rotational symmetry about the *c* axis can exist in the PtSe<sub>2</sub> family of materials.<sup>13</sup> Following the predictions, evidence of type-II Dirac cones in PtSe<sub>2</sub> was soon characterized in quantum oscillations, angle-resolved photoemission spectroscopy and negative longitudinal magnetoresistance by different groups.<sup>14,17–19</sup> Investigating such topological phase transitions in Dirac semimetal materials not only offers unique opportunities for studying the fundamental properties of Fermions but also holds potential for device applications exploiting their exotic surface excitations and bulk electric, optical and vibrational properties.<sup>15</sup>

It is well-known that the application of high pressure by modifying the lattice structure can be an effective tool to tune the structure and physical properties of PtSe<sub>2</sub>.<sup>20,21</sup> The phase transitions, chemical reaction, and anharmonicity in the lattice

potential energy can be found because of the atomic and electronic arrangements under extreme conditions.<sup>22–25</sup> Furthermore, the band structures are related to their Dirac cones, which are sensitive to the out-of-plane and in-plane interactions. Although there are reports of high-pressure behavior of phonons in PtSe<sub>2</sub> on crystals using Raman spectroscopy,<sup>26–31</sup> the phonon behaviors of PtSe<sub>2</sub> at Dirac point under proper pressure are not known. Previous work in PtSe<sub>2</sub> has concentrated on X-ray diffraction studies from pressure-induced phase transitions. However, they have not found the structure transition up to 30 GPa according to the results from X-ray diffraction and electrical transport.<sup>28,32</sup> Therefore, the knowledge of the PtSe<sub>2</sub> structural stability range under conditions of variable pressures is important for such applications.

In this Letter, we establish the pressure phase diagram of the Dirac semimetal PtSe<sub>2</sub> by high-pressure Raman scattering and theoretical calculations. Both the E<sub>g</sub> and A<sub>1g</sub> Raman modes display anomalies in the phonon frequencies accompanied by abnormal evolution of their line width starting at ~4.3 GPa. The theoretical prediction indicates that the pressure can induce the appearance of type-I Dirac cones. The phonon spectra and band structure of PtSe<sub>2</sub> are investigated under

**Received:** June 12, 2020

**Accepted:** August 12, 2020

**Published:** August 12, 2020

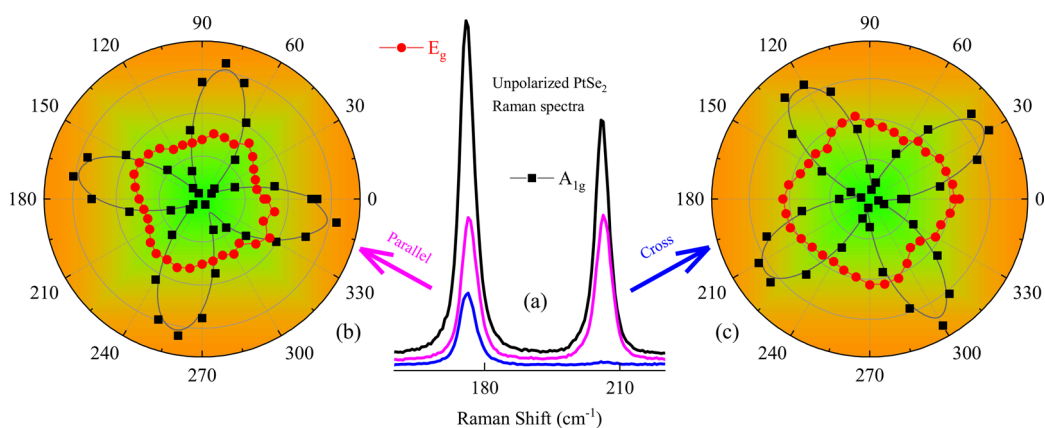


**Figure 1.** (a) Polarized Raman spectra of PtSe<sub>2</sub> single crystal measured at ambient conditions. (b) and (c) Summarized intensity of the E<sub>g</sub> and A<sub>1g</sub> modes as a function of the polarization of incidence light for parallel (red line) and cross (blue line) PtSe<sub>2</sub>.

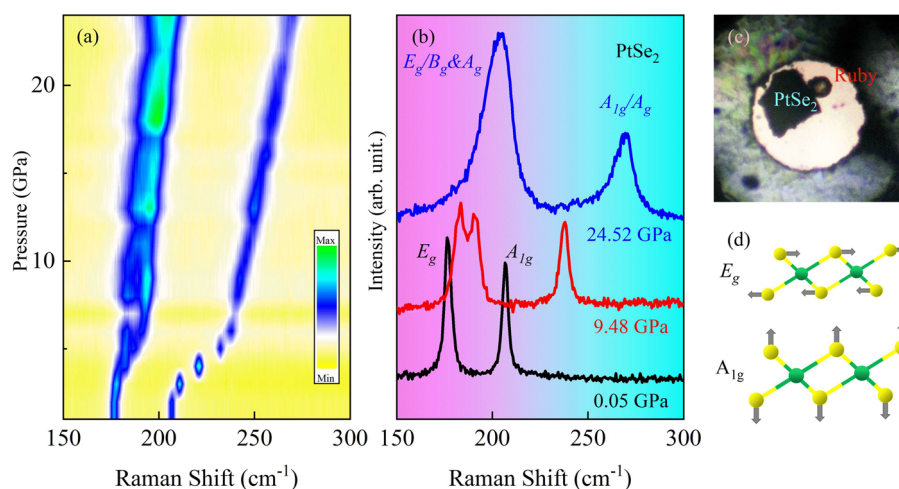


**Figure 2.** (a) Pressure maps of Raman scattering and (b) selected Raman spectra for PtSe<sub>2</sub> from ambient up to 25 GPa at room temperature. Note that each spectrum is shifted in intensity for clarity. (c) Top view of the PtSe<sub>2</sub> sample and ruby in a diamond anvil cell. (d) Schematic views of two Raman-active vibrational modes in PtSe<sub>2</sub>.

different pressures. We unambiguously determine a new pressure stabilization structure and underlying structural mechanisms of the transitions up to 25 GPa. The observation of the transition in 1T-PtSe<sub>2</sub> under high pressure provides an engineering approach to optimizing the phase as needed in applications, which not only opens up a new window for searching and controlling the phase structure and Dirac cones of the other two-dimensional materials but also promotes the practical development of reversing activity related materials and devices.<sup>33</sup>

Polarized Raman spectra measurements of the PtSe<sub>2</sub> single crystal (from 2D semiconductors) were carried out using a Jobin-Yvon LabRAM HR Evolution spectrometer (Figure 1). The sample was loaded in a Mao-Bell type diamond anvil cell (DAC) with a 300 μm culet diamond and a stainless steel gasket (Figure 2). As we know, the Raman spectra of PtSe<sub>2</sub> have higher sensitivity with the different thickness like the other two-dimensional materials.<sup>1,10,26,29,30</sup> The thickness of PtSe<sub>2</sub> is about 10 μm in our DAC for the high-pressure Raman experiment. The thickness of the PtSe<sub>2</sub> material will not change under the action of hydrostatic pressure. Thus, we can exclude the effect of thickness on our Raman spectra. Silicon oil was used as the pressure transmitting media, which maintains hydrostatic conditions up to 30 GPa. In all high-pressure

experiments, the R1-line emission of a tiny ruby was used for pressure calibration.<sup>34</sup> The polarized Raman spectra were recorded in backscattering geometry in parallel and perpendicular polarization configurations. Raman spectra were obtained by excitation with a 532 nm Nd:YAG laser beam and a 1800 grooves/mm grating. The laser beams were focused on the sample by a ×50 objective with a working distance of 18 mm. The laser was focused to a 2 μm spot with incident power on the DAC limited below 1 mW before the sample in order to reduce the laser heating effect on the surface.

The structure searching is performed by the swarm-intelligence based CALYPSO method as implemented in its same-name CALYPSO code,<sup>35–37</sup> which is based on a global minimization of free energy surfaces merging ab initio total-energy calculations. We searched for the structures of PtSe<sub>2</sub> with simulation cell sizes ranging from 1 to 4 formula units at 10 and 20 GPa, respectively. And due to the massive computational cost of predicting structures for large formula unit of PtSe<sub>2</sub>, a high-throughput screening of AB<sub>2</sub> type materials (up to 32 f.u.) is also performed on the basis of the Material Project.<sup>38</sup>

Structure optimizations and electronic calculations are performed in the framework of density functional theory<sup>39</sup> within the generalized gradient approximation<sup>40</sup> as imple-

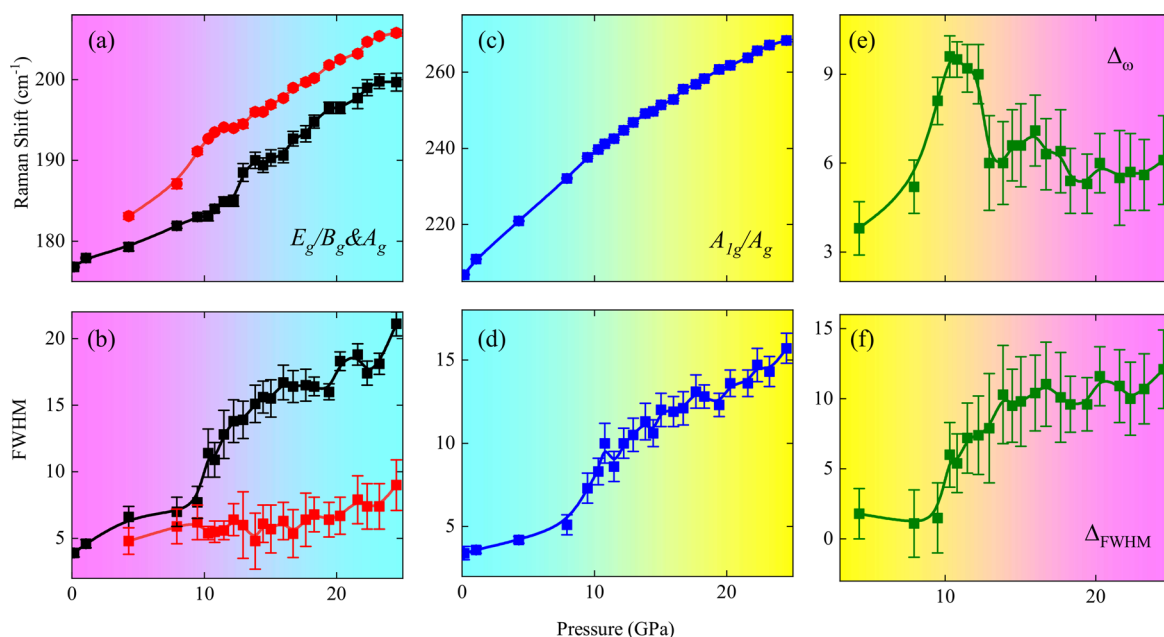


**Figure 3.** Pressure dependence of the (a), (b)  $E_g/B_g$  and  $A_g$  and (c), (d)  $A_{1g}/A_g$  Raman phonon modes from ambient pressure to 25 GPa as determined from the data of Figure 2. (e), (g) Difference of the Raman shift and fwhm for the split  $E_g/B_g$  and  $A_g$  mode, showing the phase transition regions.

mented in the VASP code.<sup>41</sup> The all-electron projector-augmented wave (PAW) method<sup>42</sup> is adopted with  $5d^96s^1$  and  $4s^24p^4$  configurations treated as the valence electrons of Pt and Se, respectively. A kinetic cutoff energy of 600 eV and the spacing of 0.2 for Monkhorst–Pack k-mesh sampling were adopted in order to ensure the enthalpy calculations converged within 1 meV/atom. The van der Waals density-functional approach (vdW-DF) with the optB86b function<sup>43</sup> is adopted in our calculations. The dynamic stability of the new structures is verified from phonon calculation using the finite displacement method as implemented in PHONOPY code.<sup>44</sup> The calculation of Raman spectrum was performed in the vaspman.py package with the VASP code as a back-end.

The optimized atomic structure of the octahedral coordination forming the 1T polytype of PtSe<sub>2</sub> belongs to  $P\bar{3}m1$  space group. For the primitive unit cell of 1T-PtSe<sub>2</sub> composed of three atoms, the phonon spectra includes nine phonons, i.e., three acoustic and six optical branches. According to the lattice dynamics analysis, the decomposition of the vibration representation of optical modes at the  $\Gamma$  point is  $\Gamma = 2E_g + 2E_u + A_{1g} + A_{2u}$  for the 1T-PtSe<sub>2</sub> structure. Optical phonon modes include two doubly degenerate in-plane vibration modes, the Raman-active  $E_g$  mode and the infrared-active  $E_u$  mode, and two single degenerate out-of-plane vibrational modes, the Raman-active  $A_{1g}$  mode and the infrared-active  $E_{2u}$  mode.

As shown in Figure 1a, the two Raman peaks  $E_g$  and  $A_{1g}$  can be observed in the experiments. The  $E_g$  mode located at  $\sim 176.3$  cm<sup>-1</sup> corresponds to an intralayer in-plane vibration of Se atoms moving in opposite directions. The  $A_{1g}$  mode located at  $\sim 206.7$  cm<sup>-1</sup> involves the out-of-plane vibration of Se atoms moving away from each other. The details of the schematic diagram of the two modes are shown in Figure 2d. The intensity of the  $E_g$  mode is higher than that of  $A_{1g}$  mode. This indicates that the  $c$ -axis motion of Se atoms has less contribution in the Raman intensity compared to the  $a$ – $b$  plane motion of the Se atoms according to the strong covalent

character between Pt and Se atoms. Figure 1 also shows the differences in the polarized and unpolarized Raman spectra of the PtSe<sub>2</sub> single crystal. All of the phonon modes are visible in the unpolarized or parallel polarization measurement, whereas in a crossed polarization Raman spectra the higher energy  $A_{1g}$  mode is vanished. Therefore, we believed that the  $A_{1g}$  mode is sensitive to polarization analysis. Figure 1b,c show the intensities of the two Raman phonon modes in polar axis. The intensity of the  $A_{1g}$  mode is polarization dependent, while the  $E_g$  mode is independent with increasing angle from 0° to 360°. According to the Raman polarization-dependent tensors, the polarization dependence of the scattering intensity expressed as  $I_s(E_g) \propto d^2$  and  $I_s(A_{1g}) \propto a^2(\cos \varphi)^2$ , where  $\varphi$  is the polarization angle of the incident light.<sup>30,45</sup> From the theoretical and polarization Raman spectra results, we confirmed the in-plane mode as  $E_g$  with polarization independence, and the out-of-plane mode as  $A_{1g}$  with polarization dependence, respectively. Note that the polarized Raman spectra show a 4-fold symmetry rather than a 2-fold symmetry such as PtS<sub>2</sub>.<sup>4,30</sup> For the  $A_{1g}$  mode under the parallel configurations, the maximum peak intensities occur at 80°, 170°, 260°, and 350° while the minimum intensities occur at 30°, 120°, 210°, and 300°. The Raman peaks under cross configurations show the opposite trend, as shown in Figure 1c. This phenomenon indicates that the peak intensities of the Raman mode are related not only to the polarization incident light angle but also to the parallel and cross configurations during the scattered lights. The highly Raman anisotropy in PtSe<sub>2</sub> enables us to investigate its physical properties as a polarization sensitive photodetector.

Parts a and b of Figure 2 display the normalized Raman spectral maps and a series of Raman spectra with selected pressures during the compression procedures. Consistent with previous reports, the two Raman phonon modes exhibit blue shifts with increasing pressure up to 25 GPa, and their intensities also simultaneously decrease. The pressure coefficients for the two modes are clearly different, especially for

Table 1. Detailed Lattice Structure of PtSe<sub>2</sub> with Different Symmetries

space group	lattice parameters (Å)	atoms	atomic coordinates (fractional)		
			X	Y	Z
<i>P</i> $\bar{3}$ <i>m</i> 1	$a = b = 3.78300$	Pt(1b)	0.00000	0.00000	0.50000
	$c = 4.98560$	Se(2d)	0.33333	0.66667	0.75936
	$\gamma = 120.00$	$\alpha = \beta = 90.00$			
<i>C</i> 2/ <i>m</i>	$a = 6.54610$ $b = 3.78220$	Pt(2a)	0.50000	0.50000	0.00000
	$c = 5.00470$	Se(4i)	0.83321	0.50000	0.74133
	$\beta = 90.05$	$\alpha = \gamma = 90.00$			

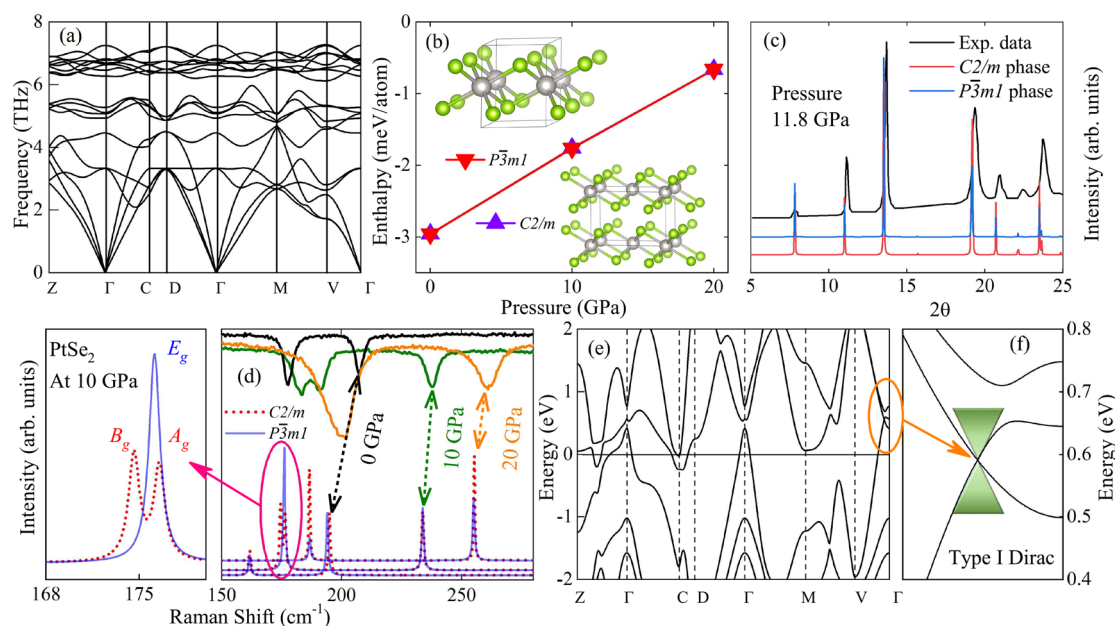


**Figure 4.** (a) Phonon spectra of the pressure stabilization structure *C*2/*m* of PtSe<sub>2</sub> at 10 GPa. (b) Calculated static energies of PtSe<sub>2</sub> with different space groups under pressure. The insets illustrate oblique view of the crystal structure of PtSe<sub>2</sub> with the *P* $\bar{3}$ *m*1 and *C*2/*m* phases. Green balls are Se atoms, and gray balls are Pt atoms. (c) Experimental and calculated XRD results of PtSe<sub>2</sub> at high pressure. (d) Experimental (upper) and calculated (lower) Raman spectra under different pressures for the PtSe<sub>2</sub> single crystal. The solid lines are the *P* $\bar{3}$ *m*1 phase and the dotted lines are the *C*2/*m* phase. The picture on the left is an enlarged view of the E<sub>g</sub> mode in the *P* $\bar{3}$ *m*1 phase and B<sub>g</sub> and A<sub>g</sub> modes in the *C*2/*m* phase at 10 GPa. (e) Band structure of PtSe<sub>2</sub> under 10 GPa. (f) Schematic diagram of the type-I Dirac cone in the enlarged PtSe<sub>2</sub> band structure under high pressure.

the A<sub>1g</sub> mode below 10 GPa with an abrupt anomaly. Note that the A<sub>1g</sub> mode is very sensitive to the pressure in the low-pressure region, which may link to its high mechanical property and sensor. The different sensitivity mechanism of the phonon mode can be attributed to the different changes between the interlayer distance and interatomic distance with increasing pressure. The interlayer distance decreases from 2.40 to 2.00 Å in the low-pressure range, 16.45% reduction in percentage. However, the value of the percentage is only 7.68% in the high pressure range. Moreover, the peak intensity of the E<sub>g</sub> mode relative to that of the A<sub>1g</sub> mode increases with pressure, consistent with the changes of vdW interactions in PtSe<sub>2</sub> single crystal. Interestingly, the two modes show a different scenario. The E<sub>g</sub> mode splits into two peaks at ~183 and ~191 cm<sup>-1</sup> in Figure 2b. As we know, the split Raman peak indicates the change of the lattice symmetry in PtSe<sub>2</sub>. With increasing pressure, the split two peaks have a blue shift and merge into one broader peak. The anomalous behavior can be attributed to pressure-induced structural changes and long-range Coulombic interlayer interactions.<sup>31</sup> The observation of the split double peak at low-frequency zone corresponding to E<sub>g</sub> Raman mode region of *P* $\bar{3}$ *m*1 space group suggests that there may be some changes in structure or phase. It is

unknown whether the split Raman peak still belong to the E<sub>g</sub> mode of *P* $\bar{3}$ *m*1 or not. We will predict the structures of PtSe<sub>2</sub> at high pressure using CALYPSO method and its same-name code in the discussion of the following letter. There are significant changes between the *c*-axis and interlayer distance of PtSe<sub>2</sub> single crystal with increasing the pressure according to our calculation from ambient pressure to 20 GPa. The interlayer distance is reduced by 22.1% from 2.40 to 1.87 Å with the high pressure. The bond length between Pt and Se atoms also decreases from 2.54 to 2.47 Å, only about 2.8% variations. Therefore, the pressure induced interlayer mechanical interaction is highly anisotropic for A<sub>1g</sub> mode, which is consist with the polarization Raman spectra results.

The Lorentz function is used to analyze the details vibration properties of the two modes, as presented in Figure 3. The pressure induced evolutions of E<sub>g</sub> and A<sub>1g</sub> modes are reversible, and the resulting blue shifts with pressure from 0 to 25 GPa are 23 and 62 cm<sup>-1</sup>, respectively. The continuous blue shifts of both peaks indicate the strengthened interaction between Pt and Se atoms caused by the contraction of the lattice under high pressure. The out-of-plane vibration A<sub>1g</sub> changes the strength of interlayer mechanical coupling by decreasing/increasing the interlayer distance. However, the in-plane

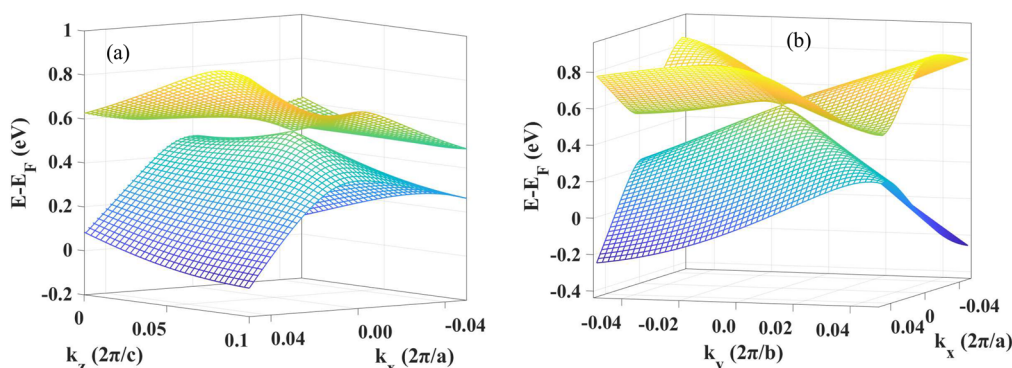


**Figure 5.** Three-dimensional band structures on the (a)  $k_y = 0$  and (b)  $k_z = 0.06$  plane around the Dirac point. The linear band crossing along three independent directions near the Dirac point confirms the type-I Dirac cone in the bulk single crystal of PtSe<sub>2</sub> under high pressure.

motion  $E_g$  only induces slight tilting of the springs, which can be driven by a much smaller force gradient.

In Figure 3, two regions corresponding to different Raman spectra can be immediately identified according to the analysis of the peak position, from ambient pressure to 10 GPa and 10–25 GPa. In the low-pressure region below 5 GPa, the  $E_g$  and  $A_{1g}$  modes are detected corresponding to the 1T phase, as confirmed in the polarization measurements. The  $E_g$  mode becomes even broader on the application of pressure and splits into two peaks above 5 GPa. The differences between the split  $E_g$  mode during compression procedures are displayed in Figure 3e,f. Furthermore, it was observed that the full width half-maximum (fwhm) increases with increasing the pressure. The  $E_g$  mode broadens from 4  $\text{cm}^{-1}$  to above 21  $\text{cm}^{-1}$ , while the  $A_{1g}$  mode broadens from 3 to 15  $\text{cm}^{-1}$ . The calculated pressure coefficients  $d_\omega(A_{1g})/d_p$  are 3.5 and 2.4  $\text{cm}^{-1} \text{GPa}^{-1}$  for the pressure below and above 5 GPa, respectively. Both the Raman peak positions and fwhm have distinct mutation phenomena between 5 and 10 GPa, which confirms the change of the lattice under the high pressure. In many other compounds, both topological quantum phase transition and Lifshitz transition can be identified by the indirect experimental results according to the anomalies Raman shifts, intensity, and fwhm under high pressure.<sup>21–23,31</sup> Upon decompression, the Raman spectral changes were partially reversible immediately and the high-pressure mixed phase fully reverted to the original structure. Therefore, according to the splitting  $E_g$  peaks and distinct mutation phenomena, a structure transition can occur by pressure and lattice distortion, resulting in a change of the point group symmetry.

As noted above, the pressure-induced change of Raman spectra demonstrates the advent of a high-pressure phase. In order to determine the structure of new phase, theoretical structure searching using CALYPSO and high-throughput screening are performed. A new pressure stabilization structure with  $C2/m$  symmetry is found, whose geometry is similar to that of 1T phase containing the PtSe<sub>2</sub> layers. The detailed lattice structure parameters and schematic diagrams of PtSe<sub>2</sub> with different symmetry are shown in Table 1 and Figure 4, respectively. In order to determine the dynamic stability, the phonon spectra of new predicted structure are also calculated, depicted in Figure 4a. The absence of any imaginary phonon frequencies in the whole Brillouin zone demonstrates that the  $C2/m$  phase is dynamically stable. Just as shown in Figure 4b, the differences of enthalpy for  $C2/m$  and  $P\bar{3}m1$  space groups are less than 1 meV/atom under pressures ranging from 0 to 20 GPa, revealing that the  $C2/m$  phase may coexist with 1T

phase. The comparison of XRD patterns between the theoretical simulations of  $C2/m$  and  $P\bar{3}m1$  space groups and experimental data at 11.8 GPa [ref 28] are presented in Figure 4c. It is evident that the difference between the  $P\bar{3}m1$  and  $C2/m$  structures is negligible.

In order to further confirm our prediction, we therefore calculated the Raman spectra of  $C2/m$  and  $P\bar{3}m1$  space groups by considering the effects of both high pressure and vdW. There are three Raman active modes  $B_g + 2A_g$  in the  $C2/m$  phase. As shown in Figure 4d, the  $B_g$  and  $A_g$  Raman modes of  $C2/m$  are degenerate and overlapped with the  $E_g$  Raman mode of  $P\bar{3}m1$  in ambient conditions. However, the  $B_g$  and  $A_g$  Raman modes of  $C2/m$  are split at pressures above 5 GPa, which has a good coincidence with the experimental results. In addition, they have a trend to degenerate again as the pressure increases beyond 15 GPa, which is also observed in the experiment. However, the  $E_g$  Raman mode in the  $P\bar{3}m1$  phase is always degenerate in the experimental pressure range. The observation of split double peaks of the  $E_g$  mode in our experiment indicates the appearance of a new phase. The split double peaks are considered to be the  $B_g$  and  $A_g$  Raman modes of the  $C2/m$  phase. As shown in Figure 3e, the difference between the low-frequency Raman mode increases during compression procedures, reaching the maximum at 10 GPa. The phase transition process is gradual rather than abrupt with increasing pressure. Then the difference decreases with increasing pressure, which leads to the observation of a large broadening peak in the low-frequency zone in the experiment. The  $B_g$  and  $B_g$  Raman modes of  $C2/m$  are indiscernible and degenerate into one peak again at 15 GPa from the theoretical simulation. Note that the energetical degeneracy of  $C2/m$  and  $P\bar{3}m1$  as well as the  $E_g$  Raman modes of  $P\bar{3}m1$  always overlapped with at least one of the  $B_g$  and  $A_g$  Raman modes of  $C2/m$  in Figure 4d. Considering the results from the Raman spectrum and energetic degeneracy, it can be concluded that  $C2/m$  and  $P\bar{3}m1$  phases can coexist under pressure.

In order to study electronic properties, we investigate band structures with the correction of spin–orbit coupling (SOC) for the new predicted  $C2/m$  phase under pressures Figure 4e. This type of material is a well-known Dirac semimetal with outstanding properties and the 1T phase of PtSe<sub>2</sub> is type-II Dirac semimetal, having been studied widely.<sup>13,19</sup> New predicted  $C2/m$  PtSe<sub>2</sub> shows a metallic property. Along the  $V-\Gamma$  direction, a type-II Dirac band crossing appears within valence bands at about 1.30 eV below the Fermi energy for  $C2/m$  PtSe<sub>2</sub> under 0 GPa, while a type-I Dirac point connecting the valence and conduction bands is found to

reside at about 0.5 eV above the Fermi energy under 10 and 20 GPa in Figure 4f. Type-I Dirac cone should have opposite slope sign and type-II Dirac cone should have the same slope sign. In order to confirm the new type-I Dirac cone in the bulk PtSe<sub>2</sub> single crystal,<sup>13</sup> the three-dimensional band structures of the C2/m phase on the  $k_y = 0$  and  $k_z = 0.06$  planes around the Dirac point have been also investigated in Figure 5a,b, respectively. It shows the linear band crossing along all the independent directions near the Dirac point in  $k$ -space. Therefore, we concluded that the high-pressure C2/m phase of PtSe<sub>2</sub> is a topological material with a type-I Dirac cone according to the calculated band structures along the three orthogonal directions from the touching point.

To summarize, we have systematically investigated the pressure dependent on structural and vibrational properties of 1T-PtSe<sub>2</sub> by Raman scattering spectroscopy and first-principles calculations. The new pressure stabilization structure C2/m is found by the theoretical prediction. The structure can be also confirmed by the anomalies in the fwhm and frequencies of Raman modes with pressure and the phonon calculation results. The type-I Dirac Fermions are found according to our band structure investigations under compression, which is associated with the emergence of the new pressure stabilization structures. The results will pave the way for detecting the phase structure of TMDs under the extreme conditions.

## AUTHOR INFORMATION

### Corresponding Authors

**Yanchao Wang** – State Key Laboratory of Superhard Materials & International Center for Computational Method and Software, Jilin University, Changchun 130012, China; [orcid.org/0000-0003-4518-925X](https://orcid.org/0000-0003-4518-925X); Phone: +86-21-54345150; Email: [wyc@calypso.cn](mailto:wyc@calypso.cn); Fax: +86-21-54342933

**Zhigao Hu** – Technical Center for Multifunctional Magneto-Optical Spectroscopy (Shanghai), Engineering Research Center of Nanophotonics & Advanced Instrument (Ministry of Education), Department of Materials, School of Physics and Electronic Science, East China Normal University, Shanghai 200241, China; Collaborative Innovation Center of Extreme Optics, Shanxi University, Taiyuan, Shanxi 030006, China; Shanghai Institute of Intelligent Electronics & Systems, Fudan University, Shanghai 200433, China; [orcid.org/0000-0003-0575-2191](https://orcid.org/0000-0003-0575-2191); Phone: +86-21-54345150; Email: [zghu@ee.ecnu.edu.cn](mailto:zghu@ee.ecnu.edu.cn); Fax: +86-21-54342933

### Authors

**Kai Jiang** – Technical Center for Multifunctional Magneto-Optical Spectroscopy (Shanghai), Engineering Research Center of Nanophotonics & Advanced Instrument (Ministry of Education), Department of Materials, School of Physics and Electronic Science, East China Normal University, Shanghai 200241, China

**Anyang Cui** – Technical Center for Multifunctional Magneto-Optical Spectroscopy (Shanghai), Engineering Research Center of Nanophotonics & Advanced Instrument (Ministry of Education), Department of Materials, School of Physics and Electronic Science, East China Normal University, Shanghai 200241, China

**Sen Shao** – State Key Laboratory of Superhard Materials & International Center for Computational Method and Software, Jilin University, Changchun 130012, China

**Jijia Feng** – Center for High Pressure Science and Technology Advanced Research, Shanghai 201203, China

**Hongliang Dong** – Center for High Pressure Science and Technology Advanced Research, Shanghai 201203, China

**Bin Chen** – Center for High Pressure Science and Technology Advanced Research, Shanghai 201203, China

**Junhao Chu** – Technical Center for Multifunctional Magneto-Optical Spectroscopy (Shanghai), Engineering Research Center of Nanophotonics & Advanced Instrument (Ministry of Education), Department of Materials, School of Physics and Electronic Science, East China Normal University, Shanghai 200241, China; Collaborative Innovation Center of Extreme Optics, Shanxi University, Taiyuan, Shanxi 030006, China; Shanghai Institute of Intelligent Electronics & Systems, Fudan University, Shanghai 200433, China

Complete contact information is available at:

<https://pubs.acs.org/10.1021/acs.jpcllett.0c01813>

### Author Contributions

<sup>†</sup>K. Jiang, A. Cui, and S. Shao contributed equally to this work. The manuscript was written through contributions of all authors. All authors have given approval to the final version of the manuscript.

### Notes

The authors declare no competing financial interest.

## ACKNOWLEDGMENTS

This work was financially supported by the National Natural Science Foundation of China (Grants Nos. 91833303, 61974043, 61805081, 61674057, 11822404, and 11774127), the National Key Research and Development Program of China (Grants No. 2018YFB0406500, 2017YFA0303403, and 2019YFB2203400), Projects of Science and Technology Commission of Shanghai Municipality (Grant Nos. 18JC1412400, 18YF1407000, 18YF1407200, and 19S11120100), China Postdoctoral Science Foundation (2020TQ0099), and the Program for Professor of Special Appointment (Eastern Scholar) at Shanghai Institutions of Higher Learning.

## REFERENCES

- (1) Yu, X.; Yu, P.; Wu, D.; Singh, B.; Zeng, Q.; Lin, H.; Zhou, W.; Lin, J.; Suenaga, K.; Liu, Z.; Wang, Q. J. Atomically thin noble metal dichalcogenide: a broadband mid-infrared semiconductor. *Nat. Commun.* **2018**, *9*, 1545.
- (2) Avsar, A.; Ciarrocchi, A.; Pizzochero, M.; Unuchek, D.; Yazyev, O. V.; Kis, A. Defect induced, layer-modulated magnetism in ultrathin metallic PtSe<sub>2</sub>. *Nat. Nanotechnol.* **2019**, *14*, 674–678.
- (3) Okogbue, E.; Han, S. S.; Ko, T.-J.; Chung, H.-S.; Ma, J.; Shaukat, M. S.; Kim, J. H.; Kim, J. H.; Ji, E.; Oh, K. H.; Zhai, L.; Lee, G.-H.; Jung, Y. Multifunctional Two-Dimensional PtSe<sub>2</sub>-Layer Kirigami Conductors with 2000% Stretchability and Metallic-to-Semiconducting Tunability. *Nano Lett.* **2019**, *19*, 7598–7607.
- (4) Liang, Q.; Wang, Q.; Zhang, Q.; Wei, J.; Lim, S. X.; Zhu, R.; Hu, J.; Wei, W.; Lee, C.; Sow, C.; Zhang, W.; Wee, A. T. S. High-Performance, Room Temperature, Ultra-Broadband Photodetectors Based on Air-Stable PdSe<sub>2</sub>. *Adv. Mater.* **2019**, *31*, 1807609.
- (5) Noh, H.-J.; Jeong, J.; Cho, E.-J.; Kim, K.; Min, B. I.; Park, B.-G. Experimental Realization of Type-II Dirac Fermions in a PdTe<sub>2</sub> Superconductor. *Phys. Rev. Lett.* **2017**, *119*, No. 016401.
- (6) Wang, Z.; Li, Q.; Besenbacher, F.; Dong, M. Facile Synthesis of Single Crystal PtSe<sub>2</sub> Nanosheets for Nanoscale Electronics. *Adv. Mater.* **2016**, *28*, 10224–10229.
- (7) Huang, Z.; Zhang, W.; Zhang, W. Computational Search for Two-Dimensional MX<sub>2</sub> Semiconductors with Possible High Electron Mobility at Room Temperature. *Materials* **2016**, *9*, 716.

- (8) Wagner, S.; Yim, C.; McEvoy, N.; Kataria, S.; Yokaribas, V.; Kuc, A.; Pindl, S.; Fritzen, C.-P.; Heine, T.; Duesberg, G. S.; Lemme, M. C. Highly Sensitive Electromechanical Piezoresistive Pressure Sensors Based on Large-Area Layered PtSe<sub>2</sub> Films. *Nano Lett.* **2018**, *18*, 3738–3745.
- (9) Kandemir, A.; Akbali, B.; Kahraman, Z.; Badalov, S. V.; Ozcan, M.; Iyikanat, F.; Sahin, H. Structural, electronic and phononic properties of PtSe<sub>2</sub>: from monolayer to bulk. *Semicond. Sci. Technol.* **2018**, *33*, No. 085002.
- (10) Yim, C.; McEvoy, N.; Riazimehr, S.; Schneider, D. S.; Gity, F.; Monaghan, S.; Hurley, P. K.; Lemme, M. C.; Duesberg, G. S. Wide Spectral Photoresponse of Layered Platinum Diselenide-Based Photodiodes. *Nano Lett.* **2018**, *18*, 1794–1800.
- (11) Hu, D.; Zhao, T.; Ping, X.; Zheng, H.; Xing, L.; Liu, X.; Zheng, J.; Sun, L.; Gu, L.; Tao, C.; Wang, D.; Jiao, L. Unveiling the Layer-Dependent Catalytic Activity of PtSe<sub>2</sub> Atomic Crystals for the Hydrogen Evolution Reaction. *Angew. Chem., Int. Ed.* **2019**, *58*, 6977–6981.
- (12) Wang, Y.; Li, L.; Yao, W.; Song, S.; Sun, J. T.; Pan, J.; Ren, X.; Li, C.; Okunishi, E.; Wang, Y.-Q.; Wang, E.; Shao, Y.; Zhang, Y. Y.; Yang, H.-t.; Schiwer, E. F.; Iwasawa, H.; Shimada, K.; Taniguchi, M.; Cheng, Z.; Zhou, S.; Du, S.; Pennycook, S. J.; Pantelides, S. T.; Gao, H.-J. Monolayer PtSe<sub>2</sub>, a New Semiconducting Transition-Metal-Dichalcogenide, Epitaxially Grown by Direct Selenization of Pt. *Nano Lett.* **2015**, *15*, 4013–4018.
- (13) Huang, H.; Zhou, S.; Duan, W. Type-II Dirac fermions in the PtSe<sub>2</sub> class of transition metal dichalcogenides. *Phys. Rev. B: Condens. Matter Mater. Phys.* **2016**, *94*, 121117.
- (14) Zhang, K.; Yan, M.; Zhang, H.; Huang, H.; Arita, M.; Sun, Z.; Duan, W.; Wu, Y.; Zhou, S. Experimental evidence for type-II Dirac semimetal in PtSe<sub>2</sub>. *Phys. Rev. B: Condens. Matter Mater. Phys.* **2017**, *96*, 125102.
- (15) Bahramy, M. S.; Clark, O. J.; Yang, B. J.; Feng, J.; Bawden, L.; Riley, J. M.; Marković, I.; Mazzola, F.; Sunko, V.; Biswas, D.; Cooil, S. P.; Jorge, M.; Wells, J. W.; Leandersson, M.; Balasubramanian, T.; Fujii, J.; Vobornik, I.; Rault, J. E.; Kim, T. K.; Hoesch, M.; Okawa, K.; Asakawa, M.; Sasagawa, T.; Eknapakul, T.; Meevasana, W.; King, P. D. C. Ubiquitous formation of bulk Dirac cones and topological surface states from a single orbital manifold in transition-metal dichalcogenides. *Nat. Mater.* **2018**, *17*, 21.
- (16) Li, Y.; Xia, Y.; Ekahana, S. A.; Kumar, N.; Jiang, J.; Yang, L.; Chen, C.; Liu, C.; Yan, B.; Felser, C.; Li, G.; Liu, Z.; Chen, Y. Topological origin of the type-II Dirac fermions in PtSe<sub>2</sub>. *Phys. Rev. Mater.* **2017**, *1*, No. 074202.
- (17) Xiao, R. C.; Gong, P. L.; Wu, Q. S.; Lu, W. J.; Wei, M. J.; Li, J. Y.; Lv, H. Y.; Luo, X.; Tong, P.; Zhu, X. B.; Sun, Y. P. Manipulation of type-I and type-II Dirac points in PdTe<sub>2</sub> superconductor by external pressure. *Phys. Rev. B: Condens. Matter Mater. Phys.* **2017**, *96*, No. 075101.
- (18) Yang, H.; Schmidt, M.; Süß, V.; Chan, M.; Balakirev, F. F.; McDonald, R. D.; Parkin, S. S. P.; Felser, C.; Yan, B.; Moll, P. J. W. Quantum oscillations in the type-II Dirac semi-metal candidate PtSe<sub>2</sub>. *New J. Phys.* **2018**, *20*, No. 043008.
- (19) Li, Z.; Zeng, Y.; Zhang, J.; Zhou, M.; Wu, W. Observation of negative longitudinal magnetoresistance in the type-II Dirac semimetal PtSe<sub>2</sub>. *Phys. Rev. B: Condens. Matter Mater. Phys.* **2018**, *98*, 165441.
- (20) Mao, H.-K.; Chen, X.-J.; Ding, Y.; Li, B.; Wang, L. Solids, liquids, and gases under high pressure. *Rev. Mod. Phys.* **2018**, *90*, No. 015007.
- (21) Gao, C.; Li, R.; Zhong, M.; Wang, R.; Wang, M.; Lin, C.; Huang, L.; Cheng, Y.; Huang, W. Stability and Phase Transition of Metastable Black Arsenic under High Pressure. *J. Phys. Chem. Lett.* **2020**, *11*, 93–98.
- (22) Pawbake, A.; Bellin, C.; Paulatto, L.; Béneut, K.; Biscaras, J.; Narayana, C.; Late, D. J.; Shukla, A. Pressure-Induced Phase Transitions in Germanium Telluride: Raman Signatures of Anharmonicity and Oxidation. *Phys. Rev. Lett.* **2019**, *122*, 145701.
- (23) O'Neal, K. R.; Cherian, J. G.; Zak, A.; Tenne, R.; Liu, Z.; Musfeldt, J. L. High Pressure Vibrational Properties of WS<sub>2</sub> Nanotubes. *Nano Lett.* **2016**, *16*, 993–999.
- (24) Liu, G.; Yu, Z.; Liu, H.; Redfern, S. A. T.; Feng, X.; Li, X.; Yuan, Y.; Yang, K.; Hirao, N.; Kawaguchi, S. I.; Li, X.; Wang, L.; Ma, Y. Unexpected Semimetallic BiS<sub>2</sub> at High Pressure and High Temperature. *J. Phys. Chem. Lett.* **2018**, *9*, 5785–5791.
- (25) Sereika, R.; Park, C.; Kenney-Benson, C.; Bandaru, S.; English, N. J.; Yin, Q.; Lei, H.; Chen, N.; Sun, C.-J.; Heald, S. M.; Ren, J.; Chang, J.; Ding, Y.; Mao, H.-k. Novel Superstructure-Phase Two-Dimensional Material 1T-VSe<sub>2</sub> at High Pressure. *J. Phys. Chem. Lett.* **2020**, *11*, 380–386.
- (26) Yan, M.; Wang, E.; Zhou, X.; Zhang, G.; Zhang, H.; Zhang, K.; Yao, W.; Lu, N.; Yang, S.; Wu, S.; Yoshikawa, T.; Miyamoto, K.; Okuda, T.; Wu, Y.; Yu, P.; Duan, W.; Zhou, S. High quality atomically thin PtSe<sub>2</sub> films grown by molecular beam epitaxy. *2D Mater.* **2017**, *4*, No. 045015.
- (27) Pawar, M. S.; Late, D. J. Temperature-dependent Raman spectroscopy and sensor applications of PtSe<sub>2</sub> nanosheets synthesized by wet chemistry. *Beilstein J. Nanotechnol.* **2019**, *10*, 467–474.
- (28) An, C.; Chen, X.; Zhou, Y.; Zhou, Y.; Zhang, B.; Chen, C.; Yuan, Y.; Zhang, R.; Zhang, L.; Zhu, X.; Yang, Z. Structural, vibrational and electrical properties of type-II Dirac semimetal PtSe<sub>2</sub> under high pressure. *J. Phys.: Condens. Matter* **2019**, *31*, 415402.
- (29) Shi, J.; Huan, Y.; Hong, M.; Xu, R.; Yang, P.; Zhang, Z.; Zou, X.; Zhang, Y. Chemical Vapor Deposition Grown Large-Scale Atomically Thin Platinum Diselenide with Semimetal-Semiconductor Transition. *ACS Nano* **2019**, *13*, 8442–8451.
- (30) Zhao, Y.; Qiao, J.; Yu, P.; Hu, Z.; Lin, Z.; Lau, S. P.; Liu, Z.; Ji, W.; Chai, Y. Extraordinarily Strong Interlayer Interaction in 2D Layered PtS<sub>2</sub>. *Adv. Mater.* **2016**, *28*, 2399–2407.
- (31) Bhatt, S. V.; Deshpande, M. P.; Sathe, V.; Rao, R.; Chaki, S. H. Raman spectroscopic investigations on transition-metal dichalcogenides MX<sub>2</sub> (M = Mo, W; X = S, Se) at high pressures and low temperature. *J. Raman Spectrosc.* **2014**, *45*, 971–979.
- (32) Yuan, Y.-F.; Zhang, Z.-T.; Wang, W.-K.; Zhou, Y.-H.; Chen, X.-L.; An, C.; Zhang, R.-R.; Zhou, Y.; Gu, C.-C.; Li, L.; Li, X.-J.; Yang, Z.-R. Pressure-induced enhancement of optoelectronic properties in PtS<sub>2</sub>. *Chin. Phys. B* **2018**, *27*, No. 066201.
- (33) Wang, Z.; Wu, H. H.; Li, Q.; Besenbacher, F.; Li, Y.; Zeng, X. C.; Dong, M. Reversing Interfacial Catalysis of Ambipolar WSe<sub>2</sub> Single Crystal. *Adv. Sci.* **2020**, *7*, 1901382.
- (34) Mao, H. K.; Xu, J.; Bell, P. M. Calibration of the ruby pressure gauge to 800 kbar under quasi-hydrostatic conditions. *J. Geophys. Res.* **1986**, *91*, 4673–4676.
- (35) Wang, Y.; Lv, J.; Zhu, L.; Ma, Y. Crystal structure prediction via particle-swarm optimization. *Phys. Rev. B: Condens. Matter Mater. Phys.* **2010**, *82*, No. 094116.
- (36) Wang, Y.; Lv, J.; Zhu, L.; Ma, Y. CALYPSO: A method for crystal structure prediction. *Comput. Phys. Commun.* **2012**, *183*, 2063–2070.
- (37) Gao, B.; Gao, P.; Lu, S.; Lv, J.; Wang, Y.; Ma, Y. Interface structure prediction via CALYPSO method. *Sci. Bull.* **2019**, *64*, 301–309.
- (38) Jain, A.; Ong, S. P.; Hautier, G.; Chen, W.; Richards, W. D.; Dacek, S.; Cholia, S.; Gunter, D.; Skinner, D.; Ceder, G.; Persson, K. A. Commentary: The Materials Project: A materials genome approach to accelerating materials innovation. *APL Mater.* **2013**, *1*, No. 011002.
- (39) Kohn, W.; Sham, L. J. Self-Consistent Equations Including Exchange and Correlation Effects. *Phys. Rev.* **1965**, *140*, A1133–A1138.
- (40) Perdew, J. P.; Chevary, J. A.; Vosko, S. H.; Jackson, K. A.; Pederson, M. R.; Singh, D. J.; Fiolhais, C. Atoms, molecules, solids, and surfaces: Applications of the generalized gradient approximation for exchange and correlation. *Phys. Rev. B: Condens. Matter Mater. Phys.* **1992**, *46*, 6671–6687.
- (41) Kresse, G.; Furthmüller, J. Efficient iterative schemes for ab initio total-energy calculations using a plane-wave basis set. *Phys. Rev. B: Condens. Matter Mater. Phys.* **1996**, *54*, 11169–11186.

(42) Blöchl, P. E. Projector augmented-wave method. *Phys. Rev. B: Condens. Matter Mater. Phys.* **1994**, *50*, 17953–17979.

(43) Wang, Y.; Wang, J. J.; Wang, W. Y.; Mei, Z. G.; Shang, S. L.; Chen, L. Q.; Liu, Z. K. A mixed-space approach to first-principles calculations of phonon frequencies for polar materials. *J. Phys.: Condens. Matter* **2010**, *22*, 202201.

(44) Togo, A.; Oba, F.; Tanaka, I. First-principles calculations of the ferroelastic transition between rutile-type and CaCl<sub>2</sub>-type SiO<sub>2</sub> at high pressures. *Phys. Rev. B: Condens. Matter Mater. Phys.* **2008**, *78*, 134106.

(45) Wang, Y.; Cong, C.; Qiu, C.; Yu, T. Raman Spectroscopy Study of Lattice Vibration and Crystallographic Orientation of Monolayer MoS<sub>2</sub> under Uniaxial Strain. *Small* **2013**, *9*, 2857–2861.